

Article

Study on the Adsorption Properties and Mechanisms of CO on Nickel Surfaces Based on Density Functional Theory

Kun Wang^{1,2,3,*}, Kunlun Li^{1,2,4} and Fuqing Wang^{1,2,4}

¹ National Frontiers Science Center for Industrial Intelligence and Systems Optimization, Northeastern University, Shenyang 110819, China

² Key Laboratory of Data Analytics and Optimization for Smart Industry, Northeastern University, Ministry of Education, Shenyang 100819, China

³ Research Institute, Shandong Iron and Steel Group, Jinan 250101, China

⁴ School of Metallurgy, Northeastern University, Shenyang 110819, China

* Correspondence: wangkun@mail.neu.edu.cn

Abstract: In this work, the adsorption of CO onto the surface of the transition metal Ni at different coverage levels was explored based on the density functional theory (DFT). The corresponding periodic slab plate models were established, and the adsorption parameters and CO electronic states on different nickel surfaces under different coverage (0.11 mL, 0.25 mL and 0.5 mL) were calculated. The results showed that the most stable adsorption sites on Ni (111) and Ni (100) crystal surfaces were valley sites, while the most stable adsorption sites on a Ni (110) surface was a short bridge site. By comparing the energy of the same adsorption sites, it was found that the adsorption of CO on a Ni (100) crystal surface was superior to the other two surfaces. Furtherly, from the perspective of the electronic structure, the density of states (DOSs) of Ni atoms and CO molecules were calculated before and after adsorption. The density of states showed that the main factor of surface adsorption generation originates from hybridization among the orbitals. This article provides insight into the mechanisms of the nickel adsorption of CO.

Keywords: density functional theory; Ni crystal surface; adsorption energy; adsorption site; density of states



Citation: Wang, K.; Li, K.; Wang, F. Study on the Adsorption Properties and Mechanisms of CO on Nickel Surfaces Based on Density Functional Theory. *Energies* **2023**, *16*, 525. <https://doi.org/10.3390/en16010525>

Academic Editors: Gregory S. Yablonsky and Konstantinos Christoforidis

Received: 29 November 2022

Revised: 23 December 2022

Accepted: 26 December 2022

Published: 3 January 2023



Copyright: © 2023 by the authors. Licensee MDPI, Basel, Switzerland. This article is an open access article distributed under the terms and conditions of the Creative Commons Attribution (CC BY) license (<https://creativecommons.org/licenses/by/4.0/>).

1. Introduction

In the context of modern industry, industrial emissions have become a major source of air pollution [1,2], where carbon monoxide (CO) is one of the components with a relatively high contribution to exhaust gases [3–5]. CO is mainly derived from the incomplete combustion of hydrocarbons and carbon-containing substances; industrial flue gas and automobile exhaust contain large amounts of CO. Taking iron ore sintering as an example, the mass concentration range of CO in sintered flue gas is about 5000 mg/m³–12,000 mg/m³ due to incomplete combustion. Relevant studies have shown that CO not only damages the function of the human heart, brain and respiratory system and severely damages human health but also causes photochemical smog pollution via photochemical reactions with NMHC (non-methane total hydrocarbons) and NO_x in the air [6,7]. However, compared with other pollutants, CO has not attracted enough attention. As the environmental situation becomes more and more severe, reducing CO emissions has attracted widespread attention. Because of this, the effective control and removal of CO is of great significance to human society and the ecological environment.

At present, CO reduction processes are mainly divided into three categories: source reduction, process control and terminal treatment. Compared with the other two strategies, terminal treatment is the most direct and effective method of pollution reduction.

In the process of terminal treatment, many researchers have explored a variety of methods to eliminate CO, including direct combustion, condensation, variable pressure

adsorption, catalytic oxidation, etc. The direct combustion method is simple and efficient, but the method is mainly suitable for the removal of high concentrations of waste gas. The method of condensation enables a large degree of exhaust gas purification. In this process, the higher the purification requirement, the lower the temperature of the cooling required, which will increase the degree of difficulties and the cost. As a result, the condensation method is usually used in combination with activated carbon adsorption, combustion and other purification methods. The variable pressure adsorption method is easy to operate and can be automatically controlled, but the cost of the device is high, which affects the industrial scale. Catalytic oxidation is one of the more promising methods of reducing CO because it has a large number of advantages, such as the fast rate of reaction, high removal efficiency, the short residence time of the exhaust gas and low operating costs.

Many researchers have explored various catalytic oxidation reactions, trying to find low-cost and efficient catalytic methods [8,9]. Relevant research [10–13] has been centered around two components: (i) Advanced catalytic oxidation technologies, including plasma, vacuum ultraviolet photolysis and catalytic ozonation technologies, which greatly enhance catalytic efficiency by introducing active factors through advanced oxidation means. However, these methods are not suitable for typical industries represented by sintered flue gas due to the difficulty and cost of operation. (ii) The exploration or development of new catalysts for different substances, which can accelerate the reaction process by reducing the activation energy of the reaction. To reduce CO in sintering flue gas, studies on traditional catalytic technology mainly focus on the research and development of new catalysts. Reasonable and efficient catalysts can reduce costs and improve catalytic efficiency. Regarding the selection of catalysts, transitional metals such as Ni, Ru, Fe, Co, Pd, Pt [14], Rh, Cr and their oxides are generally preferred [15–18]. The noble metal Ru has the best low-temperature catalytic activity of all catalysts, but it is too expensive to be widely used in the industry. Metallic iron is easy to prepare and inexpensive, but the operating temperature is high, and the catalytic activity is relatively low, while Ni-based catalysts, as typical transition metal catalysts, have high reactivity, high stability, good selectivity and are inexpensive, making them one of the most promising catalysts for current applications.

Previously, the research process of the traditional catalytic oxidation method was mainly based on physics and chemistry experiments. The surface catalytic reaction mechanism is of great significance in improving the catalyst and increasing the reaction rate. The use of the transition metal Ni for the adsorption of CO molecules is currently receiving extensive attention [19–22]. Yun et al. investigated the effect of chemisorbed CO, O, or H on the segregation behavior of the Ni element in CuNi (111) alloys. The calculated results showed that adsorbates could significantly affect the Ni segregation behavior on the CuNi (111) surface [23]. Bai et al. presented a study of adsorption structures, binding energies and so on for the adsorption of atomic species and molecular species and found that all these decomposition reactions were superior to their respective molecular desorption rates [24]. Mitchell et al. [25] explored the main pathways of CO hydrogenation reactions over Ni catalysts. They found that the CO molecular vibration frequencies on the Ni (111) surface were not well correlated with the adsorption of H atoms. Bromfield et al. [26] and Scheijen et al. [27], explored the activation energy of CO dissociation on the Ni (100) surfaces of Fe and Mo at 0.25 and 0.5 mL, respectively. For the specific location of CO molecules adsorbed on a Ni (110) crystal face, Mahaffy [28] suggested that CO molecules were adsorbed at the long bridge site. In contrast, Haq [29] showed that topside adsorption predominated when the coverage was below the 0.8 monolayer. From different perspectives, researchers still have different conclusions on the same issue. In addition, the above study only investigated one type of Ni surface and did not carry out a comprehensive and systematic analysis. The adsorption energy of the corresponding model was calculated based on DFT, and the conclusion was drawn by comparing them. The adsorption mechanism was not explored from the perspective of a deeper electronic structure.

Based on previous research results, this paper will systematically and comprehensively analyze the adsorption situation of CO on different crystal surfaces of the transition metal

Ni. The stable adsorption structure of CO adsorbed on Ni surfaces was studied based on the atomic layer number, bond length change and adsorption energy. Combined with molecular dynamics [30], relevant models were established to explore information about the corresponding preferential adsorption surface and adsorption site according to the calculation results. In light of the research results, we can select a better adsorption surface as the research object to calculate the density of the states of related atoms and molecules from the perspective of atomic orbits. Furthermore, according to the changes in the electronic structure before and after adsorption, we can determine the root cause of adsorption. Understanding the adsorption structure and density of states of CO on Ni surfaces at the atomic level is the key to studying the related catalytic reaction mechanism. It is also of great significance for the further study of gas catalytic reaction mechanisms.

2. Computational Model and Parameter-Setting

All calculations in this work are based on DFT [31–34]. The correlated energy of electronic exchange in the form of the GGA/PBE function is used in the electronic structure calculations, where the spin state of electrons needs to be considered because of the magnetic material properties of nickel. Seven-layer nickel atoms are used to simulate different surface structures. The cutoff energy is set to 520 eV. The self-consistent iterative loop convergence criterion is set to 1×10^{-6} , and the ion step relaxation convergence standard is set to -0.01 . The conjugate gradient method is chosen for the ion step relaxation algorithm. The optimized model of Ni structure cell and CO molecule is shown in Figure 1.

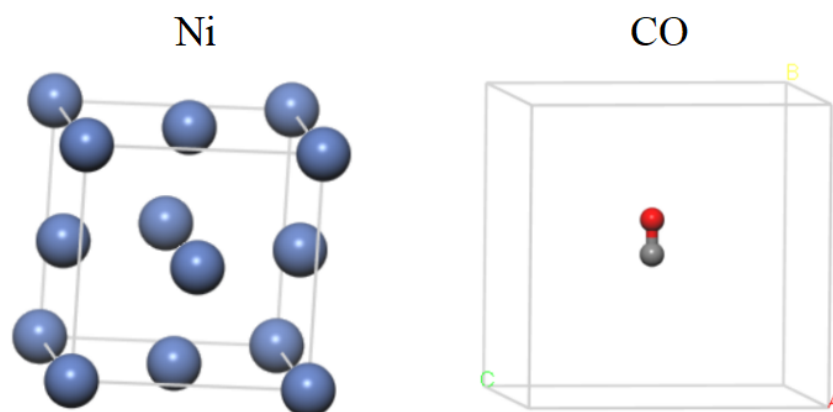


Figure 1. Optimized bulk Ni cell and CO molecule.

The Ni cell is structurally optimized with K-points of $7 \times 7 \times 7$. The lattice parameter of Ni after optimization is 3.520 Å, approaching the experimental value of 3.524 Å [35]. According to the experiment, the bond length of the C-O bond is 1.128 Å [36–38], and the simulation result is 1.143 Å. The two values are similar, which indicates that the chosen method and parameter settings are reliable. A series of tests of cutoff energy and K-point sampling were carried out before the formal start of the calculation, and the results demonstrate that the calculation parameters reach convergent conditions.

Nickel metal has a face-centered cubic structure, and three different crystal surfaces of (111), (100) and (110) were selected to explore the adsorption sites. The three neighboring atoms of the Ni (111) surface are located at exactly three vertices of an equilateral triangle. The distance between adjacent atoms is 2.489 Å, and the Ni (111) face generally undergoes only atomic relaxation without reconfiguration. The four adjacent atoms on the surface of Ni (100) form a square with 2.489 Å between adjacent atoms. Furthermore, the four adjacent atoms on the surface of Ni (110) form a rectangular surface. To meet the requirement of periodic boundary conditions for DFT calculations and to ensure that the intermolecular forces are sufficiently small, a vacuum layer of 15 Å in thickness is set to separate the supercells. In addition, considering the influence of surface relaxation on the adsorbate (CO), only some of the bottom atoms need to be fixed so that the upper atoms can relax,

which can reduce the computational effort while maintaining the accuracy of the calculation. The models are then optimized on the structure, and the adsorption energy of each model is then explored to select the better adsorption site.

The stability of adsorption is expressed by the magnitude of the molecular adsorption energy, which can be defined by the following equation:

$$E_{\text{ad}} = -\frac{1}{n}(E_{\text{CO}_{\text{ad}}} - E_{\text{surf}} - nE_{\text{CO}}) \quad (1)$$

where $E_{\text{CO}_{\text{ad}}}$ is the total energy generated by the adsorption of carbon monoxide molecules and nickel atoms, eV. E_{surf} is the energy of the cell plane, eV. E_{CO} is the energy of an isolated carbon monoxide molecule in a vacuum, eV. E_{ad} is the energy after carbon monoxide molecules are adsorbed on the surface, eV.

Coverage is a relatively important physical quantity in surface science, represented by the character S :

$$S = \frac{n}{N} \quad (2)$$

This is the proportion of the quantity of CO to the number of monolayer atoms on the solid surface, where n is the number of adsorbed gas molecules. In addition, N is the quantity of nickel atoms in the first layer. For example, in the system being researched, on a surface of p (2 × 2) Ni (111), if the quantity of nickel atoms in the first layer of the model is 4 and only one CO molecule is adsorbed, the coverage of CO is 0.25 mL.

3. Comparison of Adsorption Energies

3.1. Exploration of the Adsorption Ability of a Ni (111) Crystal Surface

There are four positions on the Ni (111) crystal surface, namely, the bridge sites, valley sites and top sites, of which the valley sites are further divided into two cases. In this process, CO is always adsorbed vertically on the Ni (111) crystal surface, and the adsorption conformation is displayed in Figure 2. The energy, adsorption parameters and adsorption configurations are shown in Table 1. The energies of these adsorption sites are 2.02 eV, 2.07 eV, 2.05 eV and 1.61 eV. By comparing the adsorptive energy of CO at different sites on the Ni (111) surface, it is found that CO adsorbs preferentially at the valley site, followed by the bridge site and, finally, at the top site of the nickel atom. In addition, through statistics and analysis, it is found that the length of the C-O bond is 1.143 Å in a free state. After the adsorption, the C-O bond length of all adsorption sites increases, and under this condition, the adsorption energy has a linear relationship with the length of the C-O bond.

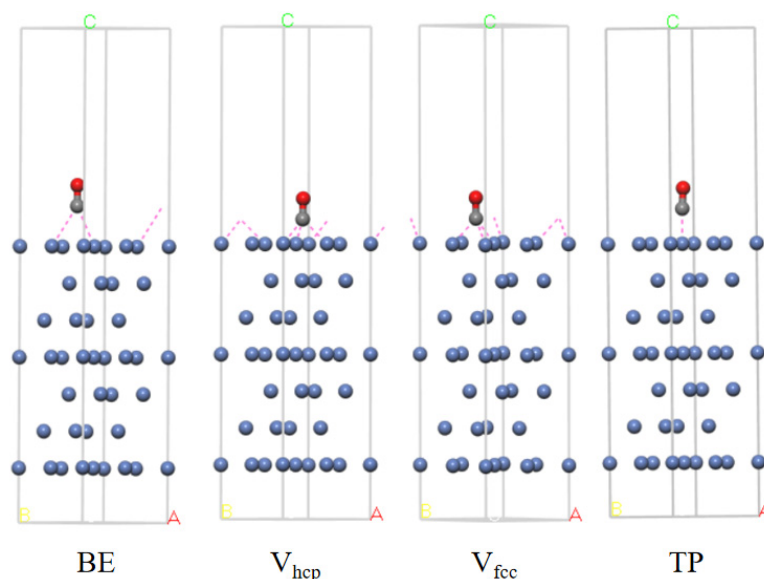


Figure 2. Four adsorption models of a CO and Ni (111) crystal surface.

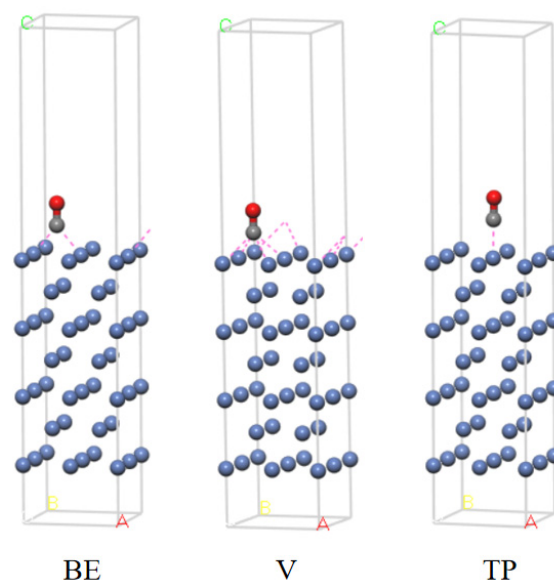
Table 1. Adsorption parameters of CO adsorption on (111), (100) and (110) surfaces at a 0.25 mL.

Surface	Site	No. of Layers	$E_{\text{CO}_{\text{ad}}}$ (eV)	E_{ad} (eV)	$d_{\text{C-O}}$ (nm)	$d_{\text{Ni-C}}$ (nm)
	CO				0.114	
Ni (111)	BE	7	−162.88	2.02	0.118	0.187
	V _{fcc}	7	−162.91	2.05	0.119	0.194
	V _{hcp}	7	−162.93	2.07	0.119	0.194
	TP	7	−162.47	1.61	0.116	0.173
Ni (100)	BE	7	−161.19	2.04	0.118	0.187
	V	7	−161.3	2.15	0.121	0.203
	TP	7	−160.94	1.79	0.116	0.173
Ni (110)	LB	7	−157.51	1.82	0.125	0.197
	SB	7	−157.71	2.05	0.118	0.187
	V	7	−157.45	1.76	0.121	0.198
	TP	7	−157.48	1.79	0.116	0.174

BE: bridge site, SB: short bridge site, LB: long bridge site, TP: top site, V: valley site.

3.2. Exploration of the Adsorption Ability of a Ni (100) Crystal Surface

There are three adsorption positions, including the bridge site, valley site and top site. The adsorptive configurations are shown in Figure 3, and the relevant data are shown in Tables 1 and 2. The data statistics and comparisons show that the Ni-C bond length is roughly distributed at 2.04 Å when CO is preferentially adsorbed at the valley site. Compared with the free state, the increasing length of the C-O bond length is 0.07 Å. This shows that when CO is at the valley sites of the Ni (100) surface it has a significant effect on the activation of CO. In addition, by analyzing the data, we can draw the conclusion that the adsorption energy of CO is weaker on the Ni (111) surface than on the Ni (100) surface at the corresponding position without changing the calculated parameters.

**Figure 3.** Three adsorption models of a CO and Ni (100) crystal surface.**Table 2.** Energy of CO in the free state and the energy of the three nickel crystal surface faces.

Scheme 111	Energy (eV)
Ni (111)	−146.08
Ni (100)	−144.37
Ni (110)	−140.91
CO	−14.78

3.3. Exploration of the Adsorption Ability of a Ni (110) Crystal Surface

Figure 4 shows four adsorption models of CO on a Ni (110) surface at 0.25 mL, and the adsorption energy, adsorption configuration and other information are listed in Table 1. These adsorption models are all seven-layer slab models, as shown in the diagram.

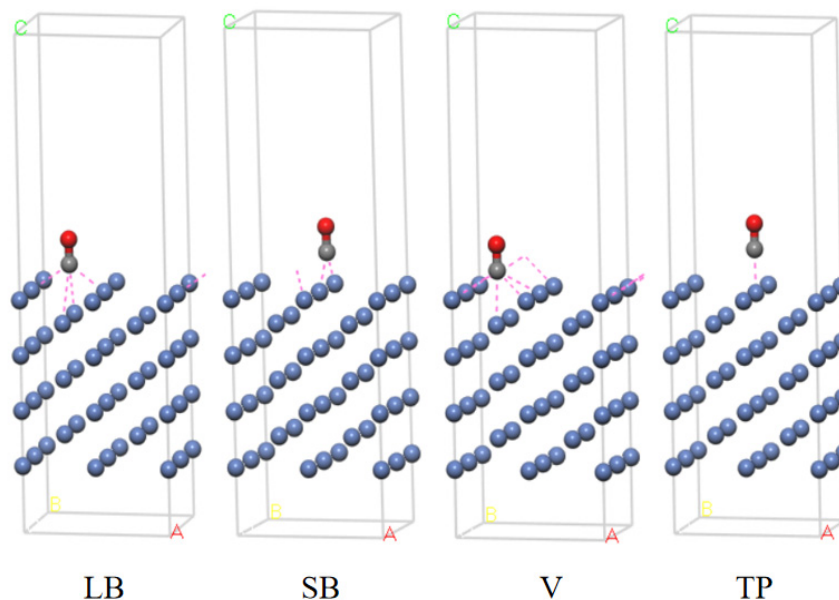


Figure 4. Four adsorption models of CO on Ni (110) crystal surface.

Initially, the number of atomic layers of the flat model is set to three. In this situation, structural optimization and calculation analysis are carried out. By comparing the models with different atomic layers, it is found that when the quantity of atomic layers is low some models are deformed, and the original morphology is changed. When the number of atomic layers is set to seven in these models, the four adsorption models mentioned above do not show any reconfiguration after structural optimization. The relevant data obtained from the calculations show that CO has the highest adsorption energy (2.05 eV) when CO is at the short bridge position of a Ni (110) crystal surface. The research results indicate that it is the most stable adsorption site for CO on the Ni (110) surface. The $d_{\text{Ni-C}}$ in this situation is 1.87 Å, and the $d_{\text{C-O}}$ is 1.18 Å, which is approximate to the results obtained by Ge et al. [39] through theoretical calculations.

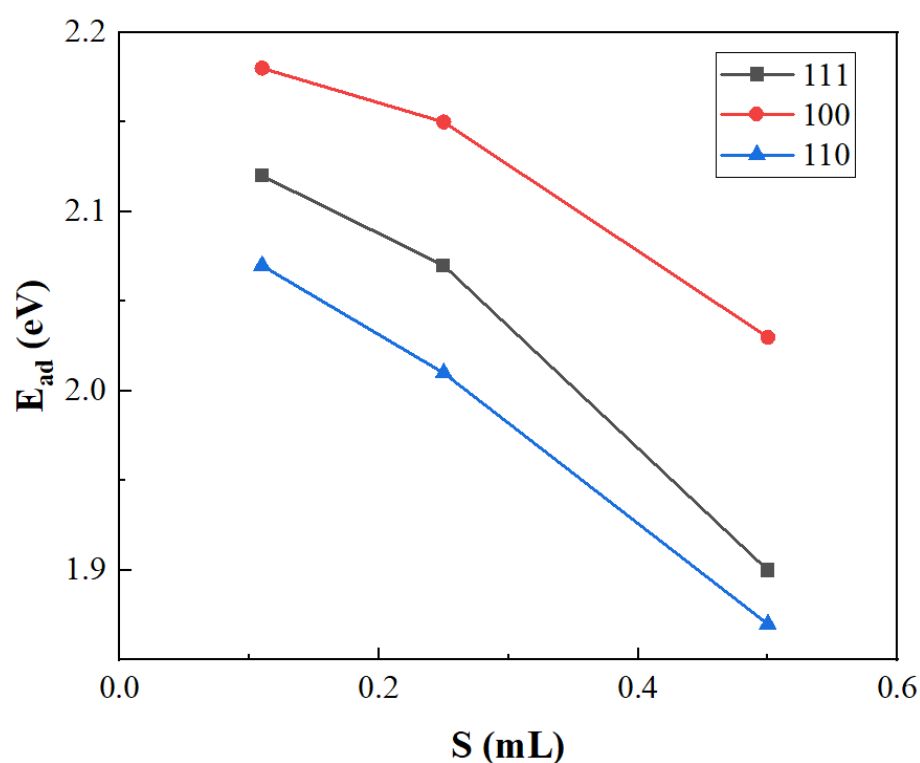
The phenomenon of reconfiguring Ni (110) crystal surfaces may be due to the change in surface balance when CO is adsorbed onto the nickel metal surface. The main objective of the current research is to explore the influence of different crystal surface configurations on the adsorption properties, so we will not investigate the changes. In addition, a comparison of the three-layer and seven-layer atomic layer data shows that the adsorption energy will be weakened when the crystal plane is reconstructed.

3.4. Influence of Coverage on CO Adsorption

At this research stage, the structural parameters of different adsorption positions are closely related to the absorption ability. When exploring the influence of coverage on adsorption performance, we mainly select the most stable adsorption positions at different crystal planes for research and analysis. In addition, we select the coverage levels of 0.11 mL, 0.25 mL and 0.5 mL. In these conditions, the adsorption positions on different crystal planes are kept the same, and structural optimization and numerical analysis are carried out. The relevant data of CO adsorption on any surfaces at three coverage degrees is shown in Table 3. For a more intuitive display, the relationship between energy and coverage is shown in Figure 5.

Table 3. Adsorption parameters of CO adsorption on three surfaces at different coverage levels.

Surface \ S (mL)	111	100	111
		Energy (eV)	
0.11	2.12	2.18	2.07
0.25	2.07	2.15	2.01
0.5	1.90	2.03	1.87
		d_{C-O} (nm)	
0.11	0.1194	0.1216	0.1184
0.25	0.1192	0.1212	0.1182
0.5	0.1183	0.1200	0.1176

**Figure 5.** The variations of adsorption energy with coverage on three crystal surfaces.

The adsorption energy of CO adsorbed on three crystal surfaces of nickel is calculated separately for different coverage levels. From the calculations, we discovered that the strength of the interaction is in the order of (100) > (111) > (110) when CO is adsorbed on the surfaces of nickel with diverse coverage. And the corresponding adsorption will decrease when the coverage is increased. The results show that under certain coverage levels, the smaller the coverage level, the greater the adsorption effect. When the coverage level increases, the mutual repulsion between the CO molecules will gradually strengthen, and the adsorption effect between the CO and the surface of the Ni will weaken. Eichler also obtained the same conclusion by studying the Ni (111) surface [40].

The calculation outcomes show that the adsorption ability will be affected by the repulsion force between CO molecules. With the increase in coverage, the distance between CO molecules will become smaller, and the adsorption energy will decrease. This phenomenon may be caused by the electronic effect, which will inhibit CO from receiving electrons from Ni cells [41,42]. The conclusion that adsorption decreases with the increase in coverage can also be demonstrated by the change in the C-O bond length. The bond length in the free state of CO is 1.143 Å. When CO molecules are on the crystal plane of nickel, the

bond length of carbon monoxide will increase, and the lower the coverage, the longer the length of the CO. Still, with the increase in coverage, the length of the C-O bond shows a decreasing trend. However, it is always higher than the bond length in the free state. The details are shown in the Figure 6.

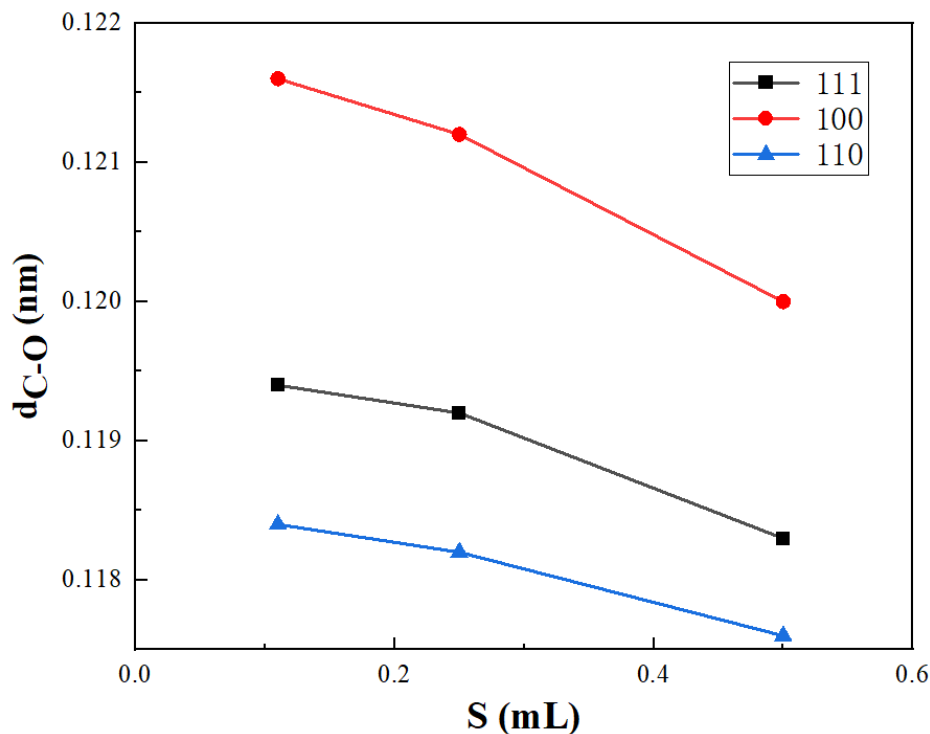


Figure 6. The variation of C-O bond lengths with coverage on three crystal surfaces.

4. The Density of State Analysis

The above calculations show that CO is preferentially adsorbed on the Ni (100) crystal surface. On account of this, the surface is used as the object of study. The change in the electronic structure in the adsorption process is studied, and the electronic density of the states of Ni and CO before and after adsorption is calculated. Figure 7 shows the changes in the density of the states of the CO and Ni before and after adsorption. As can be seen from the image, the density of the states of both the CO and Ni change before and after adsorption. Compared with that before adsorption, Ni atoms show surface electronic states in an energy range of $-10\text{ eV}\sim-8\text{ eV}$ and $-7.5\text{ eV}\sim-6\text{ eV}$. The electronic density of the states of the CO molecules change significantly before and after adsorption, and surface electronic states appear in an energy range of $-10\text{ eV}\sim-8\text{ eV}$, $-7.5\text{ eV}\sim-6\text{ eV}$ and $2\text{ eV}\sim5\text{ eV}$.

Figure 8 reveals a comparison of the density of the states of CO and Ni after adsorption. It can be seen in the figure that there is a hybrid phenomenon between them in an energy range of $-10\text{ eV}\sim-8\text{ eV}$, $-7.5\text{ eV}\sim-6\text{ eV}$ and $2\text{ eV}\sim5\text{ eV}$. Among them, in the energy range of $-10\text{ eV}\sim-8\text{ eV}$ and $-7.5\text{ eV}\sim-6\text{ eV}$, Ni atoms and CO molecules have strong hybridization, while in an energy range of $2\text{ eV}\sim5\text{ eV}$, there is no apparent hybridization between them.

The adsorption of CO molecules on the Ni crystal face leads to a change in their electronic states. In order to confirm their orbital compositions, the density of the state image is divided according to the different orbitals based on Figure 8 to obtain the atomic orbital density of the state images of carbon, oxygen and nickel atoms. Figure 9 shows the density of the states of the different orbitals of carbon, oxygen and nickel atoms after adsorption. Based on the results shown in the graphics, the hybridization of CO molecules and Ni atoms in an energy range of $-10\text{ eV}\sim-8\text{ eV}$ mainly comes from the hybridization of the s orbitals of the carbon atom and the s and p_z orbitals of the oxygen atom with the s, p and d orbitals of the nickel atom. In an energy range of $-7.5\text{ eV}\sim-6\text{ eV}$, the

surface adsorption of both produces hybridization mainly due to the hybridization of the p_x and p_y orbitals of carbon and oxygen atoms with the s and d orbitals of nickel atoms. The hybridization phenomenon in the energy range of 2 eV–5 eV arises mainly due to the hybridization of the p_x and p_y orbitals of carbon atoms with the p and d orbitals of nickel atoms.

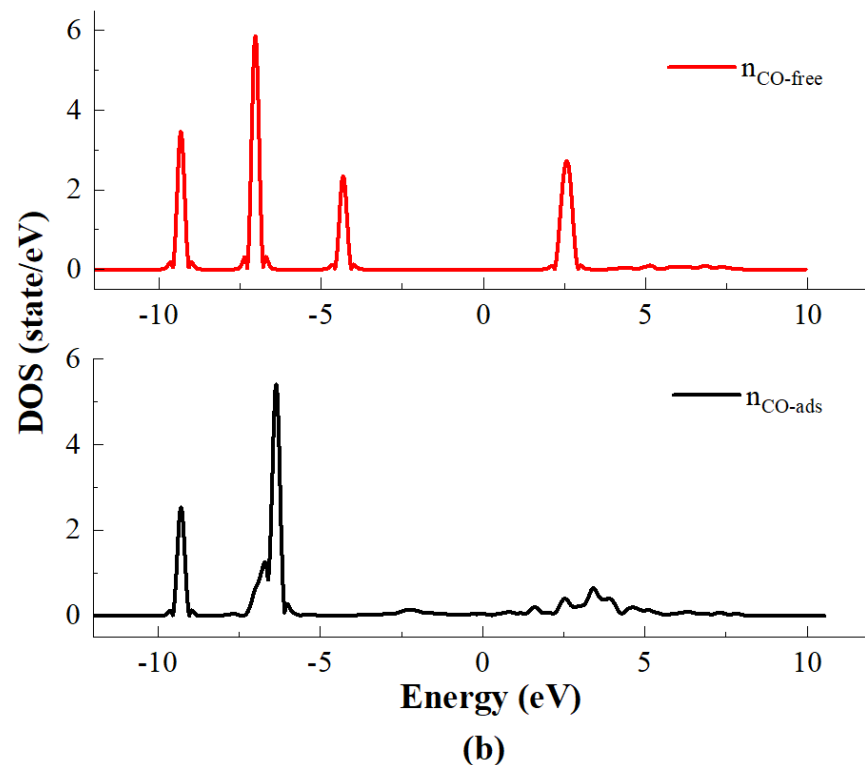
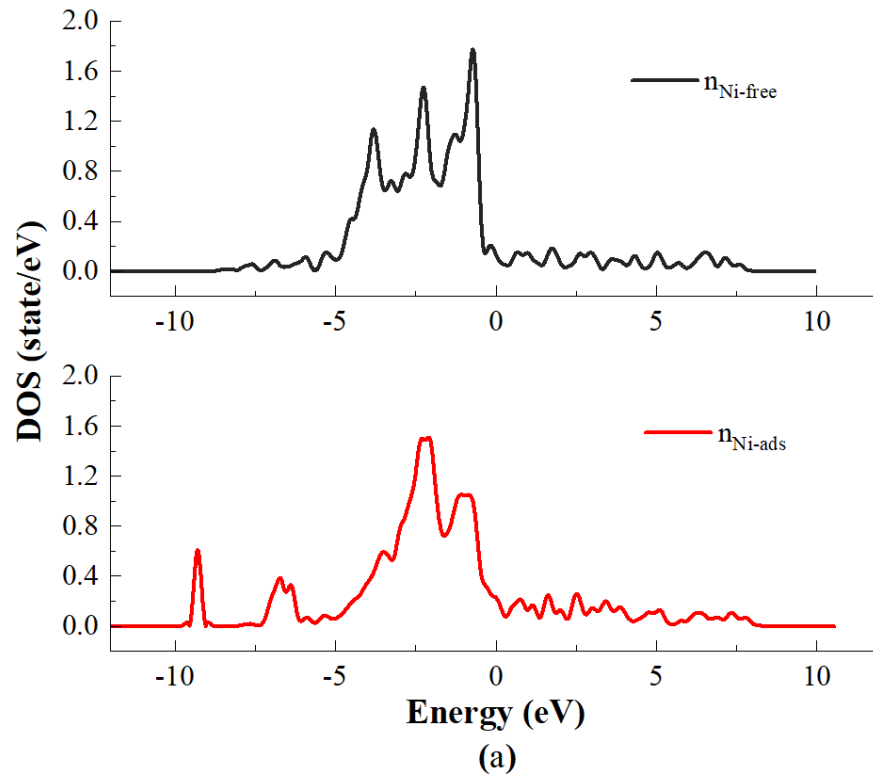


Figure 7. Electronic density of states of (a) Ni and (b) CO before and after adsorption.

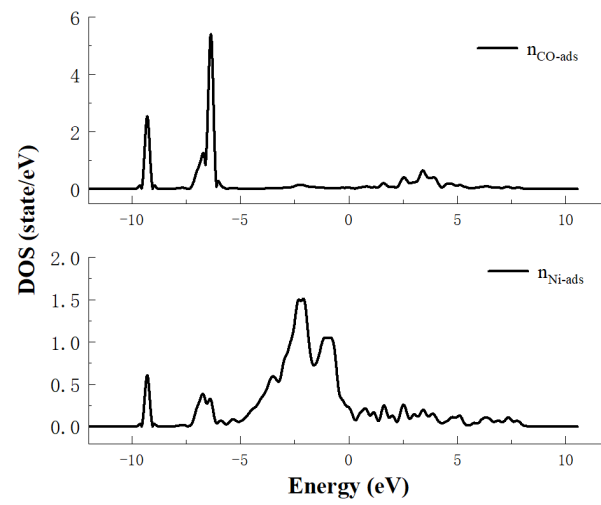


Figure 8. Comparison of the density of the states of a CO molecule and a Ni atom after adsorption.

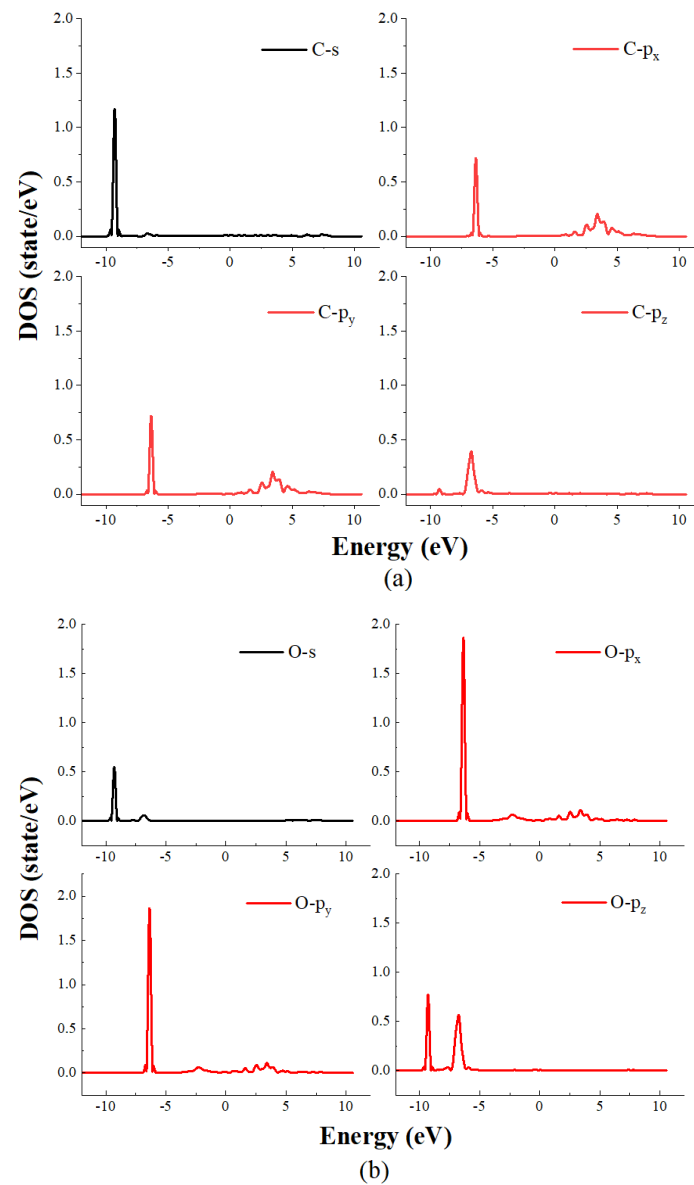


Figure 9. Cont.

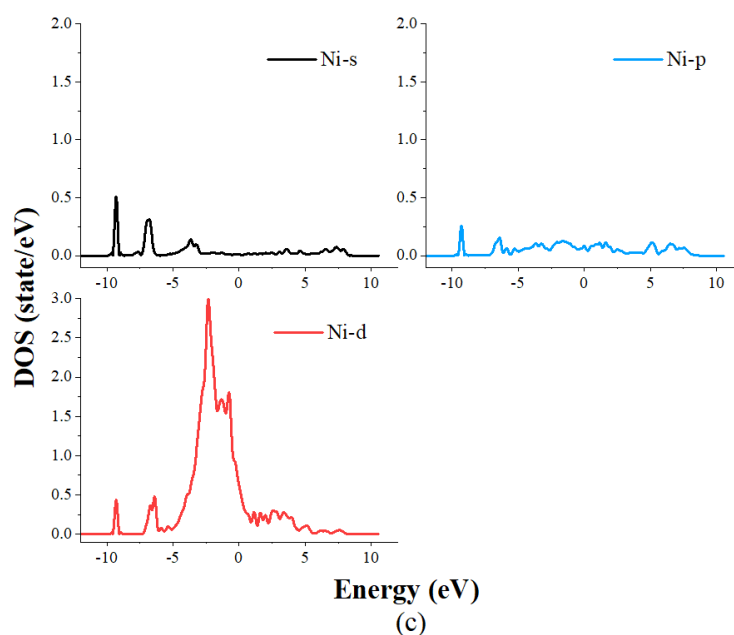


Figure 9. Density of the orbital states for each atom after adsorption: (a) carbon atom; (b) oxygen atom; (c) nickel atom.

5. Conclusions

1. By simulating and calculating the parameters of CO adsorption energy, the adsorption structure and the bond length on different crystal faces and different adsorption sites, we conclude that CO has the strongest energy at the valley position on the Ni (111) crystal surface under the four models. Similarly, the most stable adsorption position on the Ni (100) crystal surface is the valley position. Different from the former, the most substantial adsorption position on the Ni (110) crystal face under the four adsorption models is the short bridge site. CO is activated to varying degrees at all adsorption sites. At 0.11 mL, 0.25 mL and 0.5 mL, the preferential adsorption order of CO is (100) > (111) > (110).
2. When a carbon monoxide molecule is adsorbed on Ni (111) and Ni (100) crystal surfaces, the length of the C-O bond will be longer with the increase in adsorption energy. However, there is no such linear relationship when it is adsorbed on a Ni (110) crystal surface. In addition, when located at the same adsorption position, the C-O bond length decreases with the increase in coverage, and the adsorption effect becomes weaker.
3. The results of the density of states study show that the main reason for the adsorption of CO on the Ni crystal plane contains two parts: the first part is the hybridization of the s orbitals of carbon atoms and the s and p_z orbitals of oxygen atoms with the s, p and d orbitals of nickel atoms in an energy range of $-10\text{ eV}\sim-8\text{ eV}$. The second part is the hybridization of the p_x and p_y orbitals of both carbon and oxygen atoms with the s and d orbitals of nickel atoms in an energy range of $-7.5\text{ eV}\sim-6\text{ eV}$.

Author Contributions: Conceptualization, K.W.; methodology, K.W. and K.L.; software, K.L.; validation, K.L. and F.W.; formal analysis, K.W. and K.L.; investigation, K.L. and F.W.; writing—original draft preparation, K.L.; writing—review and editing, K.W. and F.W. All authors have read and agreed to the published version of the manuscript.

Funding: This research was financially supported by the National Natural Science Foundation of China (52276102); China Postdoctoral Science Foundation (2022M721970).

Data Availability Statement: Not available.

Conflicts of Interest: The authors declare no conflict of interest.

References

1. Liu, J.; Zhou, C.; Yue, W.; Yan, B.; Lin, Y.; Huang, A. Facile and green template-free synthesis of morphology-controllable Co_3O_4 catalysts for CO oxidation. *Chem. Phys. Lett.* **2020**, *756*, 137817. [[CrossRef](#)]
2. Huan, W.; Li, J.; Ji, J.; Xing, M. In situ studies on ceria promoted cobalt oxide for CO oxidation. *Chin. J. Catal.* **2019**, *40*, 656–663. [[CrossRef](#)]
3. Zheng, B.; de Beurs, K.M.; Owsley, B.C.; Henebry, G.M. Scaling relationship between CO pollution and population size over major US metropolitan statistical areas. *Landsc. Urban Plan.* **2019**, *187*, 191–198. [[CrossRef](#)]
4. Lou, Z.; Yuan, D.; Zhang, F.; Wang, Y.; Li, Y.; Zhu, L. Fe_3Si assisted Co_3O_4 nanorods: A case study of photothermal catalytic CO oxidation under ambient solar irradiation. *Nano Energy* **2019**, *62*, 653–659. [[CrossRef](#)]
5. Rezaei, P.; Rezaei, M.; Meshkani, F. Low temperature CO oxidation over mesoporous iron and copper mixed oxides nanopowders synthesized by a simple one-pot solid-state method. *Process Saf. Environ. Prot.* **2018**, *119*, 379–388. [[CrossRef](#)]
6. Ma, J.; Xu, X.; Zhao, C.; Yan, P. A review of atmospheric chemistry research in China: Photochemical smog, haze pollution, and gas-aerosol interactions. *Adv. Atmos. Sci.* **2012**, *29*, 1006–1026. [[CrossRef](#)]
7. Gavrila, C.; Ardelean, F.; Coman, A.; Burchiu, E. Statistical analysis for prognosis of a photochemical smog episode. *Model. Civ. Environ. Eng.* **2013**, *9*, 20–24. [[CrossRef](#)]
8. Miyajima, K.; Mafune, F. Catalytic reactions of gas phase zirconium oxide clusters with NO and CO revealed by post heating. *Chem. Phys. Lett.* **2016**, *660*, 261–265. [[CrossRef](#)]
9. Han, Y.-X.; Kong, C.; Hou, L.-J.; Chen, D.-P.; Wu, B.-W.; Geng, Z.-Y. Theoretical research on the catalytic reaction mechanism of N_2O and CO over Ni-5 cluster. *Comput. Theor. Chem.* **2017**, *1117*, 12–19. [[CrossRef](#)]
10. Royer, S.; Duprez, D. Catalytic oxidation of carbon monoxide over transition metal oxides. *Chemcatchem* **2011**, *3*, 24–65. [[CrossRef](#)]
11. Feng, C.; Liu, X.; Zhu, T.; Tian, M. Catalytic oxidation of CO on noble metal-based catalysts. *Environ. Sci. Pollut. Res.* **2021**, *28*, 24847–24871. [[CrossRef](#)] [[PubMed](#)]
12. Patel, D.M.; Kodgire, P.; Dwivedi, A.H. Low temperature oxidation of carbon monoxide for heat recuperation: A green approach for energy production and a catalytic review. *J. Clean. Prod.* **2020**, *245*, 118838. [[CrossRef](#)]
13. Ovcharov, M.L.; Granchak, V.M. Photocatalytic activation of carbon monoxide on semiconductors and derived nanocomposites: Basic principles and mechanisms: A review. *Theor. Exp. Chem.* **2019**, *55*, 173–200. [[CrossRef](#)]
14. Rao, Y.; Wu, Y.; Dai, X.; Zhang, Y.W.; Qin, G.; Qi, W.; Li, S. A tale of two sites: Neighboring atomically dispersed Pt sites cooperatively remove trace H_2 in CO-rich stream. *Small* **2022**, *18*, e2204611. [[CrossRef](#)]
15. Huo, J.; Zhang, Y.-B.; Zou, W.-Y.; Hu, X.; Deng, Q.; Chen, D. Mini-review on an engineering approach towards the selection of transition metal complex-based catalysts for photocatalytic H_2 production. *Catal. Sci. Technol.* **2019**, *9*, 2716–2727. [[CrossRef](#)]
16. Tanaka, H.; Misono, M. Advances in designing perovskite catalysts. *Curr. Opin. Solid State Mater. Sci.* **2001**, *5*, 381–387. [[CrossRef](#)]
17. Behr, A.; Henze, G.; Johnen, L.; Awungacha, C. Advances in thermomorphic liquid/liquid recycling of homogeneous transition metal catalysts. *J. Mol. Catal. A Chem.* **2008**, *285*, 20–28. [[CrossRef](#)]
18. Barkhordarian, G.; Klassen, T.; Bormann, R. Catalytic mechanism of transition-metal compounds on Mg hydrogen sorption reaction. *J. Phys. Chem. B* **2006**, *110*, 11020–11024. [[CrossRef](#)]
19. Bhargava, S.K.; Akolekar, D.B. Adsorption of NO and CO over transition-metal-incorporated mesoporous catalytic materials. *J. Colloid Interface Sci.* **2005**, *281*, 171–178. [[CrossRef](#)]
20. Canto, G.; Dzib, L.; Lanz, C.; Juan, A.; Brizuela, G.; Simonetti, S. Carbon monoxide adsorption on a nickel iron surface: Bonding and electronic structure computational study. *Mol. Phys.* **2012**, *110*, 113–120. [[CrossRef](#)]
21. Yu, X.; Jin, L.; Zhao, C.; Liu, Z. High coverage CO adsorption on Fe_6O_6 cluster using GGA plus U. *J. Clust. Sci.* **2020**, *31*, 591–600. [[CrossRef](#)]
22. Zhao, X.; Zhang, R.; Ling, L.; Wang, B. Insights into the effect of coverage on CO adsorption and dissociation over Rh(100) surface: A theoretical study. *Appl. Surf. Sci.* **2014**, *320*, 681–688. [[CrossRef](#)]
23. Yu, Y.; Liu, Z.; Huang, W.; Zhou, S.; Hu, Z.; Wang, L. Density functional theory study of Ni segregation in CuNi(111) alloy with chemisorbed CO, O, or H. *J. Phys. Chem. Solids* **2022**, *171*, 111021. [[CrossRef](#)]
24. Bai, Y.; Kirvassilis, D.; Xu, L.; Mavrikakis, M. Atomic and molecular adsorption on Ni(111). *Surf. Sci.* **2019**, *679*, 240–253. [[CrossRef](#)]
25. Mitchell, G.E.; Gland, J.L.; White, J.M. Vibrational spectra of coadsorbed CO and H on Ni(100) and Ni(111). *Surf. Sci.* **1983**, *131*, 167–178. [[CrossRef](#)]
26. Bromfield, T.C.; Ferre, D.C.; Niemantsverdriet, J.W. A DFT study of the adsorption and dissociation of CO on Fe(100): Influence of surface coverage on the nature of accessible adsorption states. *Chemphyschem* **2005**, *6*, 254–260. [[CrossRef](#)]
27. Scheijen, F.J.E.; Niemantsverdriet, J.W.H.; Ferre, D.C. Density Functional theory study of CO adsorption and dissociation on molybdenum(100). *J. Phys. Chem. C* **2007**, *111*, 13473–13480. [[CrossRef](#)]
28. Mahaffy, P.R.; Dignam, M.J. Carbon monoxide adsorption on Ni(110) studied by infrared ellipsometric spectroscopy. *Surf. Sci.* **1980**, *97*, 377–392. [[CrossRef](#)]
29. Haq, S.; Love, J.G.; King, D.A. The adsorption of CO on Ni{110} and its interaction with hydrogen: A RAIRS study. *Surf. Sci.* **1992**, *275*, 170–184. [[CrossRef](#)]
30. Sodeifian, G.; Razmimanesh, F. Diffusional interaction behavior of NSAIDs in lipid bilayer membrane using molecular dynamics (MD) simulation: Aspirin and Ibuprofen. *J. Biomol. Struct. Dyn.* **2019**, *37*, 1666–1684. [[CrossRef](#)]

31. Zhang, Y.; Huang, Y.; Chen, X.-S.; Lu, W. The study of oxygen and sulfur adsorption on the InSb (110) surface, using first-principle energy calculations. *Acta Phys. Sin.* **2013**, *62*, 206102. [[CrossRef](#)]
32. Zhao, H.; Yang, Y.; Shu, X.; Wang, Y.; Ran, Q. Adsorption of organic molecules on mineral surfaces studied by first-principle calculations: A review. *Adv. Colloid Interface Sci.* **2018**, *256*, 230–241. [[CrossRef](#)] [[PubMed](#)]
33. Delley, B. Fast calculation of electrostatics in crystals and large molecules. *J. Phys. Chem.* **1996**, *100*, 6107–6110. [[CrossRef](#)]
34. Perdew, J.P.; Wang, Y. Accurate and simple analytic representation of the electron-gas correlation energy. *Phys. Rev. B* **1992**, *45*, 13244. [[CrossRef](#)]
35. Peng, H.; Xie, Y.; Nie, Y. Electronic Structure of Ni Metal. *Mater. Rev.* **2007**, *4*, 131–134.
36. Shao, J.; Cheng, X.; Yang, X.; Zhang, F.; Ge, S. Calculations of bond dissociation energies and bond lengths of C-H, C-N, C-O, N-N. *J. At. Mol. Phys.* **2006**, *23*, 80–84.
37. Xi, Y.-J.; Li, Y.; Wu, D.; Li, Z.-R. Theoretical study of the COLin complexes: Interaction between carbon monoxide and lithium clusters of different sizes. *Comput. Theor. Chem.* **2012**, *994*, 6–13. [[CrossRef](#)]
38. Gross, L.; Mohn, F.; Moll, N.; Schuler, B.; Criado, A.; Guitian, E.; Pena, D.; Gourdon, A.; Meyer, G. Bond-Order Discrimination by Atomic Force Microscopy. *Science* **2012**, *337*, 1326–1329. [[CrossRef](#)]
39. Ge, Q.; Jenkins, S.J.; King, D.A. Localisation of adsorbate-induced demagnetisation: CO chemisorbed on Ni{110}. *Chem. Phys. Lett.* **2000**, *327*, 125–130. [[CrossRef](#)]
40. Eichler, A. CO adsorption on Ni(111)—A density functional theory study. *Surf. Sci.* **2003**, *526*, 332–340. [[CrossRef](#)]
41. Inderwildi, O.R.; Lebedez, D.; Deutschmann, O.; Warnatz, J. Coverage dependence of oxygen decomposition and surface diffusion on rhodium (111): A DFT study. *J. Chem. Phys.* **2005**, *122*, 034710. [[CrossRef](#)] [[PubMed](#)]
42. Wang, S.G.; Cao, D.B.; Li, Y.W.; Wang, J.G.; Jiao, H.J. Chemisorption of CO₂ on nickel surfaces. *J. Phys. Chem. B* **2005**, *109*, 18956–18963. [[CrossRef](#)] [[PubMed](#)]

Disclaimer/Publisher’s Note: The statements, opinions and data contained in all publications are solely those of the individual author(s) and contributor(s) and not of MDPI and/or the editor(s). MDPI and/or the editor(s) disclaim responsibility for any injury to people or property resulting from any ideas, methods, instructions or products referred to in the content.